Civil and Environmental Engineering
Vol. 0, Issue 0, DOI: 10.2478/cee-2026-0073

Analysis of the Influence of Different Geometric Parameters on Residual Stress of Top Plate-U Ribs

Yue CHEN[1,2], Qiuhe LI[3], Zhenyu ZHANG[2], Peiwen SHEN[4,*], Wenyu QIU[2], Ying GU[2]

[1] State Key Laboratory of Mountain Bridge and Tunnel Engineering, Chongqing Jiaotong University, Chongqing 400074, China.

[2] School of Civil Engineering, Chongqing Jiaotong University, Chongqing 400074, China.

[3] China Construction Eighth Engineering Division Corp., Ltd. South China Branch, China.

[4] Chongqing University of Education, Chongqing 400065, China.

* corresponding author: shenpw@cque.edu.cn

Date of Submission: 22 September 2025
Revision Date: 26 November 2025
Date of Acceptance: 17 December 2025

Civil and Environmental Engineering
Journal of the Faculty of Civil Engineering | University of Žilina

Abstract

Residual stress significantly affects the structural safety of steel bridge decks. This study investigates the influence of key geometric parameters, including top plate thickness, bevel angle, and the height and thickness of U ribs, on welding-induced residual stress through numerical simulation. First, in ABAQUS, the welding heat source is applied to the weld seam using the “life and death” element technique and a Dflux subroutine to obtain the temperature field. Next, the temperature field data are applied as external loads in a coupled stress field analysis to characterize the residual stress distribution, with parametric modeling used to examine the effects of varying geometric parameters. Finally, regression analysis using SPSS identifies the sensitivity of each parameter. The results show that increasing the top plate thickness reduces the maximum tensile stress near the weld but has little effect on residual stress in regions distant from the weld; increasing the bevel angle from 46° to 52° raises the peak longitudinal residual stress from 455 MPa to 520 MPa, although this effect decreases with distance from the weld; increasing U rib height reduces peak stress at the weld, while thicker U ribs result in a more uniform stress distribution. Regression analysis confirms that top plate thickness and bevel angle are the most influential factors affecting residual stress. These findings provide a quantitative basis for optimizing the design and welding process of steel bridge deck U rib structures.

Keywords

Top Plate-U Ribs; Weld residual stress; Geometry parameters; Influencing factors.

1. Introduction

Residual stress in the structural details of steel bridges is a critical factor influencing bridge service safety (McCLUNG, 2007; Tabatabaeian, 2022; Liu, 2024; Odrobiňák, 2025). Previous studies have demonstrated that the residual stress field not only significantly reduces the fatigue performance of welded components (Van den Berg, 2021; Zhang, 2022; Van Pham, 2024; Chen, 2025) and promotes the early initiation and propagation of micro-cracks, but also interacts with external loads, producing a superimposed effect that causes the actual stress level to far exceed the design threshold. This phenomenon severely limits the load-bearing capacity and service life of steel bridges (Cui, 2019; Gadallaha, 2020). In practical engineering, longitudinal ribs of orthotropic steel decks commonly adopt U rib stiffening details. However, due to the complex coupling between geometric parameters and the resulting residual stress distribution (Shim, 1992; Wang, 2023; Chen, 2025), most existing studies focus on single-parameter analyses and often overlook the correlations among different geometric parameters. Consequently, the regulatory mechanism by which geometric parameters influence the residual stress field remains insufficiently understood (Liang, 2022; Li, 2024; Bora, 2024). This research gap greatly hinders the systematic optimization of fatigue performance in the structural details of long-span steel bridge decks. To address these limitations, this study aims to enhance the fatigue performance of long-span steel bridge decks by establishing a design-oriented methodology for regulating welding-induced residual stress through the coordinated optimization of key geometric parameters.

2. The numerical simulation of residual stress in top plate-U ribs

2.1. The simulation of temperature field

Establishment of the welding model

This study is based on the actual construction of a steel bridge located in Jiangsu Province. A finite element model of the top plate-U rib welded joint was developed to analyze the welding-induced residual stress in this critical structural detail. The schematic diagram of the numerical model and the weld configuration is shown in Fig. 1.

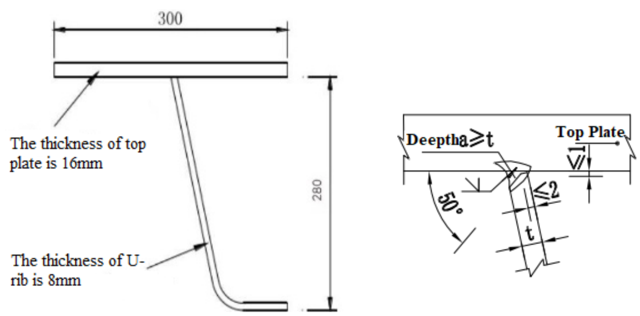

Figure1: Schematic diagram of the numerical model and weld configuration

Thermal parameters of the materials

Table 1 summarizes the thermophysical and mechanical parameters of Q345 steel used in the analysis.

Table 1: Thermophysical and mechanical parameters of Q345 steel

Temp [°C]	k [W/(m·K)]	P [kg/m^3]	C_{TE} [1/°C]	E [MPa]	v	YS [MPa]	C [J/(kg·°C)]
20	50	7850	0.000011	205000	0.28	345	460
100	49	7850	1.05E-05	197000	0.28	310	465
250	47	7850	1.22E-05	187000	0.29	275	480
500	40	7850	1.39E-05	150000	0.31	240	575
750	27	7850	1.48E-05	70000	0.35	40	625
1000	30	7850	1.35E-05	20000	0.4	20	675
1500	35	7850	1.33E-05	100	0.45	1	650
2000	145	7859	1.31E-05	1	0.48	1	820

Note: k is thermal conductivity, ρ is density, C_{TE} is the coefficient of thermal expansion, E is Young's modulus, v is Poisson's ratio, YS is yield strength, and c represents specific heat capacity.

The thermal properties of materials have long been a key challenge in welding heat transfer analysis. Due to experimental limitations and testing constraints, the currently available thermal data for structural steels remain insufficient and incomplete. To address this issue, the thermophysical properties of the materials were fully considered in this study. Based on preliminary work, the missing data were supplemented and optimized through interpolation and appropriate derivation techniques.

Mesh generation of the numerical model

To improve the accuracy of the numerical analysis, hexahedral elements were adopted throughout the model. Most regions were meshed using structured grids, while the areas with significant changes in geometric density were meshed using swept grids combined with the Advancing Front algorithm. In the simulation, mesh density control was applied to refine the grids: the element size in the weld seam was set to 1 mm, gradually increasing from 1 mm to 2 mm with distance from the weld, and reaching a maximum of 6 mm at the farthest region. This strategy ensures a more uniform element distribution and maintains high consistency between the mesh structure and the seed-point arrangement, thereby improving the overall accuracy of the simulation. The finite element model of the top plate-U rib structure is shown in Fig. 2.

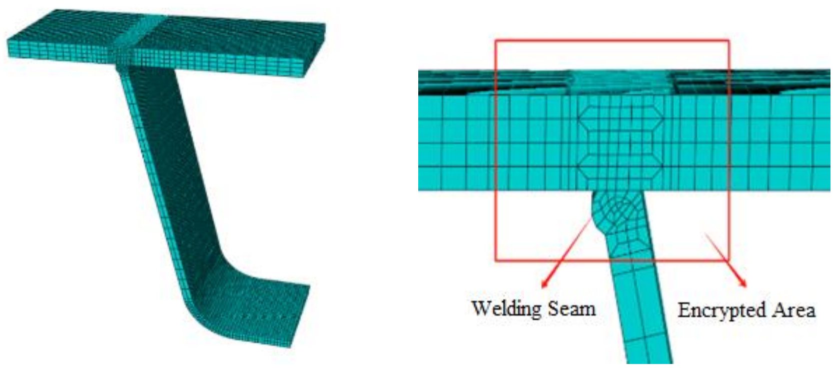

Figure 2: Finite element model of the top plate-U rib

Definition of thermal boundary conditions

Before applying thermal boundary conditions, functional grouping of the discretized meshes was conducted according to the simulation objectives. Differentiated constraint parameters were then assigned to each subdomain to accurately capture the dynamic thermal response associated with material phase transformation and surface morphology evolution during welding. The initial ambient temperature was uniformly set to 20 °C, consistent with conventional laboratory conditions. Under the action of the heat source, heat is transferred within the structure, a process that must be mathematically characterized by establishing a convective heat transfer model. The calibration of the convective heat transfer coefficient therefore becomes a key control parameter (Mondal, 2021; Nascimento, 2023; Boussaq, 2025). For the thermal radiation boundary, an emissivity of 0.75 was applied, while the Stefan-Boltzmann constant was set to 5.67×10^{-8} W/($m^2\cdot K^4$), and the absolute zero temperature was defined as −273.15 °C. The combination of convection and radiation boundary conditions enables the model to capture the transient thermal behavior during material activation and accurately reflect the energy exchange between the weld interface and the surrounding environment, thereby ensuring the authenticity of the simulated temperature field.

The selection and loading of heat source

Because ABAQUS does not directly support dynamic loading and movement of a welding heat source, Visual Studio was coupled with ABAQUS, and a user-defined DFLUX subroutine was developed in Fortran to implement the heat-source loading and motion. The design and implementation process of the DFLUX subroutine is illustrated in Fig. 3, where x_0 represents the initial coordinate and d denotes the displacement of the moving heat source.

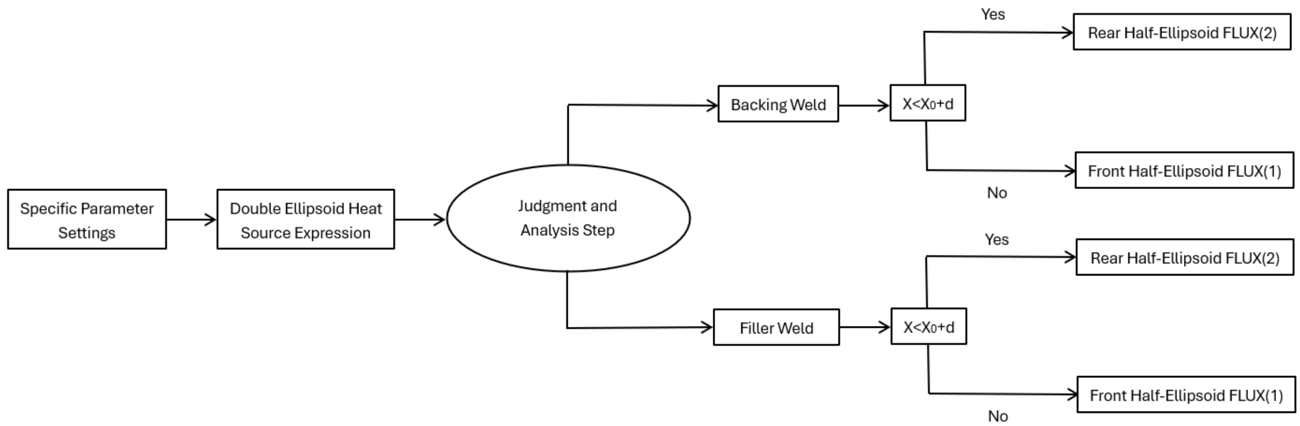

Figure 3: Design diagram of the DFLUX subroutine

During the development of this subroutine, a series of welding process parameters must be specified (Djoković, 2015; Yu, 2023; Gu, 2024), including thermal efficiency, welding speed, initial welding coordinates, welding current, voltage, and the geometric parameters of the double-ellipsoid heat source (e.g., length, width, depth). The specific ranges of these parameters are listed in Table 2.

Table 2: Parameters of the double-ellipsoid heat source

f_1 [-]	f_2 [-]	a_1 [-]	a_2 [-]	b [-]	c [-]	v [mm/s]	U [V]	I [A]	η [-]
0.67	1.43	3.5	12	3.5	8	8	220	24	0.75

Note: f_1 and f_2 are heat distribution coefficients; a_1, a_2, b, and c are geometric parameters of the double-ellipsoid heat source; v is the heat-source travel speed; U is the welding voltage; I is the welding current; η is the effective thermal efficiency of the welding arc.

Control of analysis steps

In this study, a welding model for the top plate-U rib structure was established. The total weld length was set to 100 mm, and a welding speed of 8 mm/s was applied for double-pass welding. The welding duration of each pass was therefore 12.5 s, resulting in a total welding time of 25 s for both passes. To achieve a refined simulation, the weld path was divided into 80 elements along the welding direction, and the thermal load application time for each element was controlled with a temporal resolution of 0.15625 s. After the welding process, a forced cooling period of 300 s was applied to the first weld pass, while the cooling time for the second weld pass was extended to 3000 s. This configuration forms a complete welding thermal cycle with a total duration of 3025 s.

2.2. The verification of temperature field

To investigate the temperature distribution along the weld more accurately, several time points were selected to analyze the temperature evolution at the weld center of both the first and second weld passes (along the weld direction). Fig. 4(a) illustrates the temperature distribution along the center of the first weld pass at 3 s, 6 s, and 9 s, while Fig. 4(b) presents the temperature distribution along the center of the second weld pass at 316 s, 320 s, and 324 s.

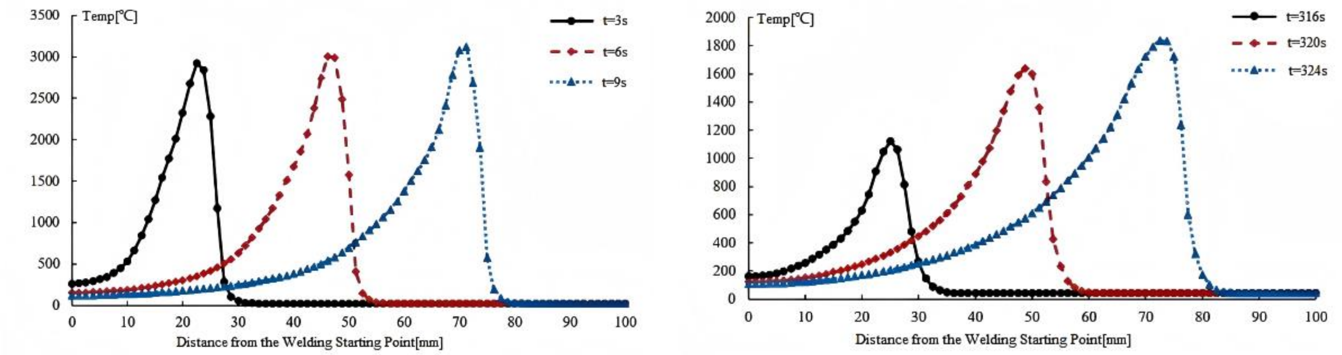

(*a*) First weld pass (*b*) Second weld pass

Figure 4: Temperature variation along the weld center at different time points

During the welding process, the temperature evolution along the weld center exhibits a consistent trend, as shown in Fig. 4. As the distance to the heat-source center decreases, the temperature gradually increases and reaches a peak within the region directly affected by the heat source. For the first weld pass, a relatively stable peak temperature is maintained at different time points. For the second weld pass, peak temperatures are also observed, but a more pronounced temperature rise occurs due to the delayed heat input. Both the root pass and filler pass exhibit quasi-steady-state temperature distributions, which show strong agreement with theoretical expectations. Overall, the numerical model for the top plate-U rib welding demonstrates good engineering applicability. The heat-source loading method, analysis procedure, and mesh design are effectively validated by the consistency between the simulated temperature evolution and the actual heat-transfer behavior observed in welding.

2.3. Results of the temperature field

A multi-dimensional temperature-field characterization method was established for the welding simulation of the top plate-U rib. By collecting complete thermal-cycle data throughout the welding process, the temporal evolution of temperature gradients was analyzed in detail.

Within the 100-mm weld length, five monitoring nodes were arranged at equal intervals along the weld direction, located 20 mm, 40 mm, 60 mm, 80 mm, and 100 mm from the welding start point. The temperature-time histories obtained from these nodes provide essential support for validating the spatial accuracy of the heat-source model. The locations of the five measurement points along the weld direction are shown in Fig. 5.

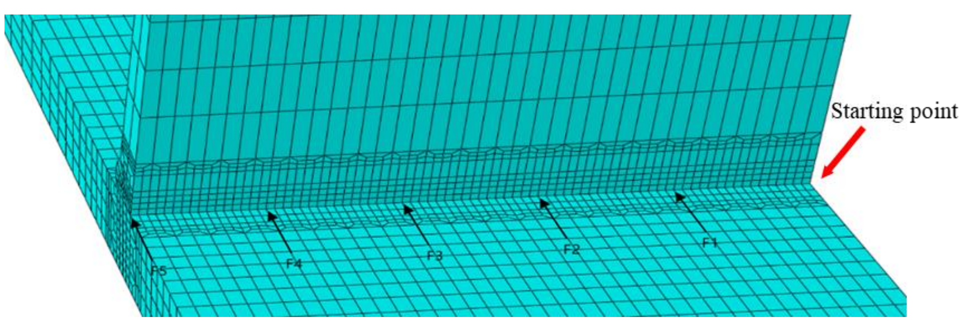

Figure 5: Arrangement of monitoring points along the weld direction

The temperature fields at the five measurement points (F1-F5) along the weld direction over time are shown in Fig. 6.

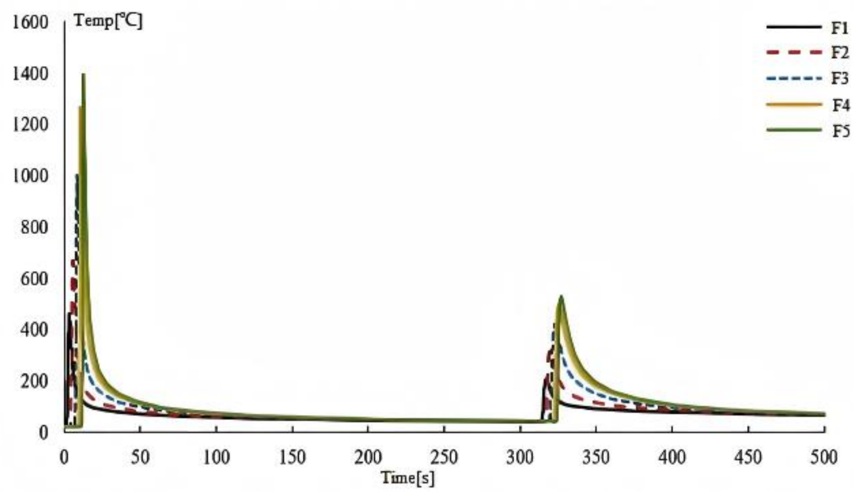

Figure 6: Temperature-time curves of the measurement points along the weld direction

From Fig. 6, it can be observed that during welding, the temperature at each measurement point reaches its maximum when the heat source passes over it, and then gradually decreases as the heat source moves away. The temperature variation is more pronounced when the heat source approaches a measurement point, while the rate of change significantly diminishes after the heat source has passed. In addition, point F1 reaches its peak temperature earlier than all other points, and its peak value is relatively lower. This is because F1 is located at the start end of the weld, where the temperature field is still in its initial development stage, whereas the other points experience a quasi-steady-state temperature field.

Five monitoring nodes were also arranged beneath the top plate in the direction perpendicular to the weld. These measurement points were located 2 mm, 4 mm, 4.77 mm, 7 mm, and 8.18 mm from the weld center, as illustrated in Fig. 7.

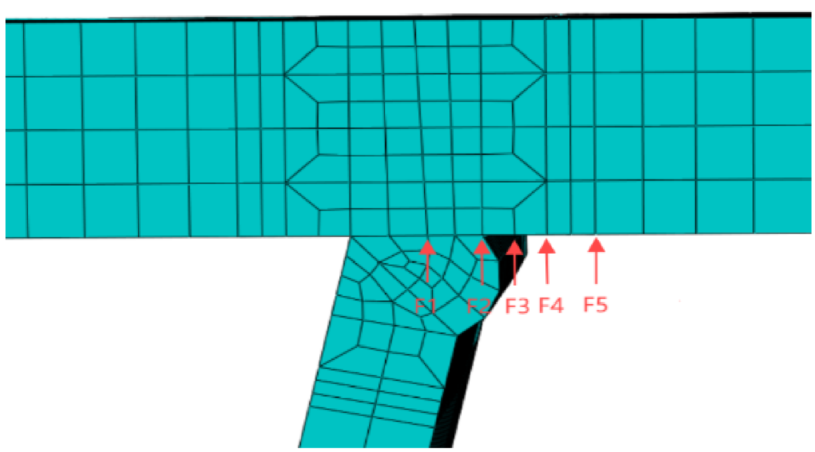

Figure 7: Arrangement of monitoring points perpendicular to the weld direction

The temperature fields at the five measurement points (F1-F5) perpendicular to the weld direction over time are shown in Fig. 8.

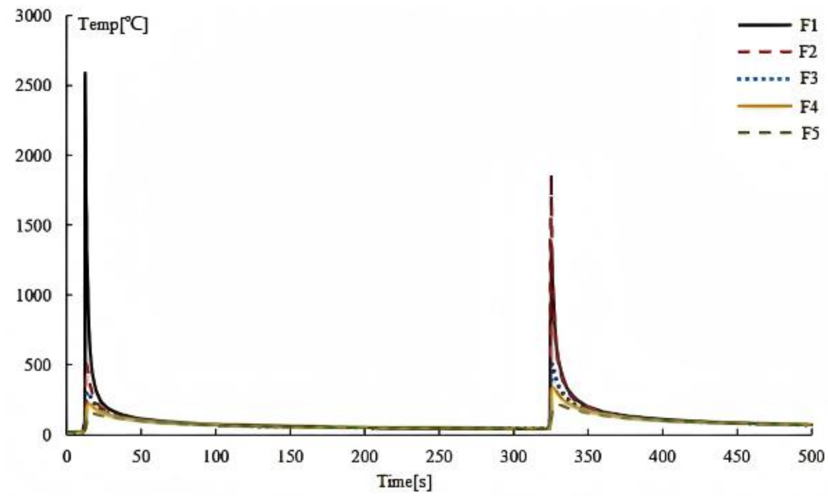

Figure 8: Temperature-time curves of the measurement points perpendicular to the weld direction

From Fig. 8, it can be seen that as the heat source progresses, the temperature at each measurement point rises rapidly and reaches its peak. Once the heat source moves away, the temperature begins to decrease, the cooling rate gradually slows, and eventually the temperature stabilizes at ambient conditions. Because the model involves two weld passes, two distinct temperature peaks appear in the temperature-time curves. For point F1, the peak temperature of the first weld pass is higher than that of the second pass, as F1 is closer to the heat-source center during the first welding process. In contrast, for points F2 through F5, the peak temperature of the second weld pass exceeds that of the first pass because these points are located closer to the heat-source center during the second welding. Moreover, the peak temperature decreases progressively with increasing distance from the weld center.

2.4. Simulation of the stress field

Determination of material parameters and element types

In the temperature-field analysis, only three thermal parameters are required: thermal conductivity, density, and specific heat. For the stress-field analysis, three additional mechanical parameters are needed: Young's modulus, thermal expansion coefficient, and yield strength. As these six parameters have already been introduced in the temperature-field analysis, they are not repeated here. It is worth noting that the element types used for the temperature and stress analyses are different. For the stress-field simulation, 3D solid eight-node reduced-integration elements (C3D8R) were adopted.

The conditions of model boundary

In the stress-field simulation, the boundary conditions were configured to replicate the actual mechanical constraints of the top plate-U rib while avoiding over-constraint or rigid-body motion. A full-degree-of-freedom constraint was applied to the symmetry plane of the half-model, ensuring structural symmetry. Along the edges of the top plate, displacement restrictions were imposed in the positive x-direction and the negative z-direction to prevent unintended lateral and vertical movements. Additionally, a z-direction displacement constraint was applied to the vertical side of the weld to stabilize the model during loading. The coordinate system was defined with the z-axis aligned with the weld direction, the y-axis oriented perpendicular to the top plate and pointing downward, and the x-axis perpendicular to the weld. As shown in Fig. 9, yellow indicates translational constraints, while blue indicates rotational constraints. These boundary conditions ensure numerical stability and physical consistency in the stress-field analysis.

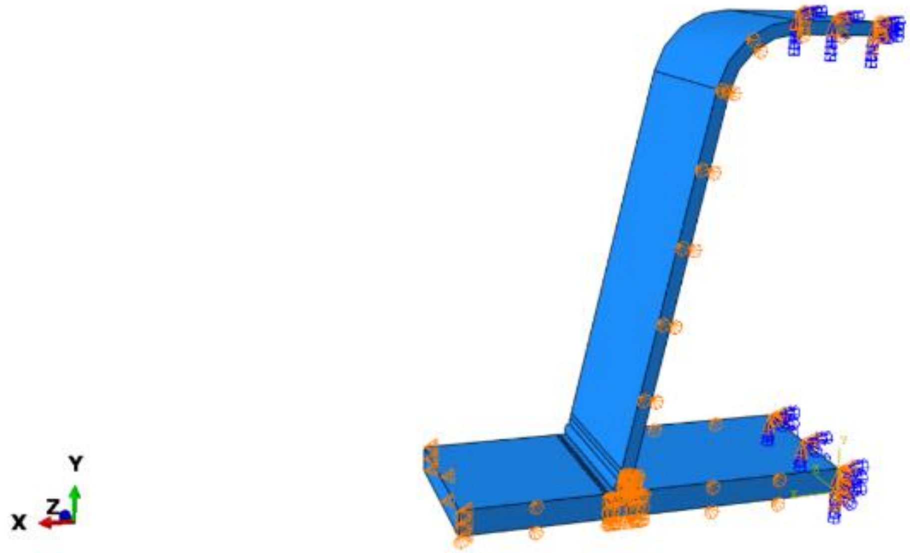

Figure 9: Diagram of boundary conditions

Application of loads and solution

The stress-field calculation is based on the previously obtained temperature-field results, which are imported into the model as external loads. Before the analysis, the initial temperature field is defined as room temperature (20 °C) to remain consistent with the temperature-field simulation. Since thermal convection and radiation are not involved in mechanical analysis, the corresponding boundary conditions used in the temperature-field calculation must be removed. The duration of the analysis steps is kept identical to that of the temperature-field simulation so that the stress-field solution can correctly inherit the thermal history. When defining the applied loads, the predefined fields must be replaced with the output file from the temperature simulation. The load application in each analysis step must be synchronized with the data sequence in the temperature-field results to ensure the accuracy of the stress-field solution.

2.5. Verification of the stress field

At this stage, the stress-field simulation has been essentially completed. Before proceeding to adjust the simulation by modifying geometric dimensions, it is necessary to verify the reliability of the current simulation results. Due to experimental limitations and potential errors in actual components, it is difficult to directly summarize the residual stress distribution laws of the top plate-U rib after welding. Therefore, verification is performed by comparing the simulation results with experimental data reported in the literature. The procedure involves replicating previous experiments in numerical simulations, performing a comparative analysis between the simulation results and experimental measurements, and thereby confirming the reliability of the current model.

Wang (2022) and Zheng (2024) conducted model tests on the top plate-U rib of a steel box girder, where partial measurement points were arranged and residual stresses of the top plate and U rib plate were measured using the blind-hole method. The test specimens were scaled down at a ratio of 1:2.5 relative to the actual dimensions. The specimen size and construction details are shown in Fig. 10.

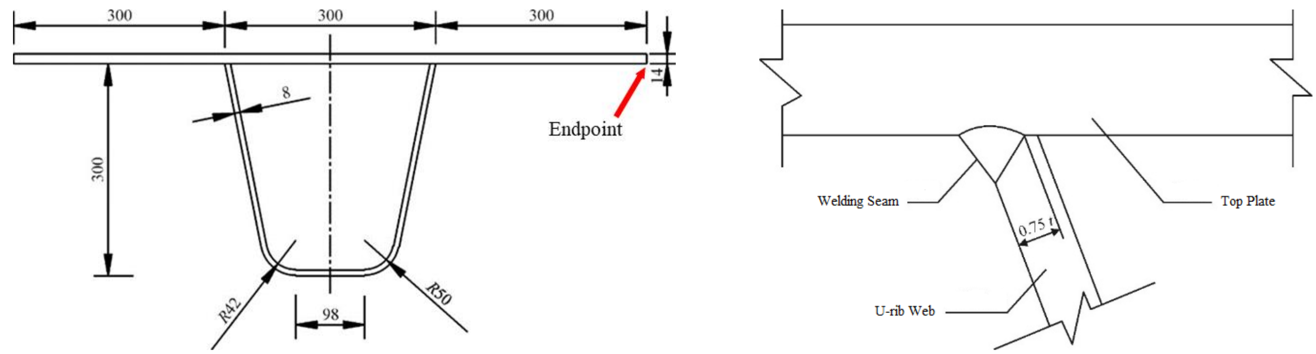

(*a*) U rib stiffened steel deck [mm] (*b*) Structural details of U rib weld with plate

Figure 10: Specimen construction details

Analysis of top plate residual stress

In this study, the actual specimen dimensions were simulated using ABAQUS 6.14, and the welding-induced residual stress was analyzed. The comparison between numerical simulation results and experimental measurements for the top plate and U rib is shown in Fig. 11.

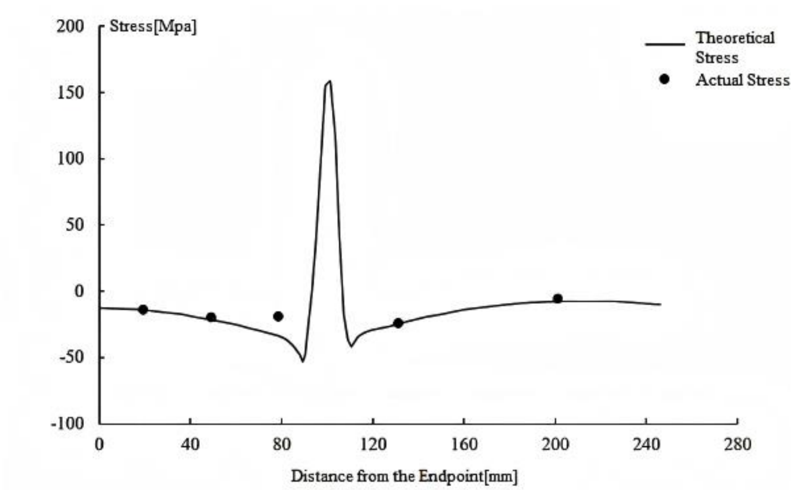

Figure 11: Comparison of simulated top plate residual stress with experimental results

As shown in Fig. 11, the longitudinal residual stress distribution obtained from the simulation closely matches the measured data in terms of overall trend. This agreement confirms the effectiveness of the numerical simulation methodology for the top plate-U rib. Some deviations are observed at certain locations, particularly near the stress peak in the central region (approximately 80-120 mm), where the simulation predicts a sharper peak than the measured values. Such discrepancies may arise from measurement errors, material heterogeneity, or boundary condition assumptions, but these deviations are generally systematic and unavoidable.

Compared to experimental measurements, numerical simulations offer broader coverage. Experimental methods cannot capture stress data at all locations across the entire structure, whereas simulations provide a more complete stress-field map. This advantage allows for more comprehensive numerical references and data support for analyzing the residual stress distribution in top plate-U ribs, thereby enhancing the scientific rigor and completeness of the study.

Analysis of residual stress in U rib plates

The longitudinal residual stress of the U rib plate and its comparison with experimental data are shown in Fig. 12.

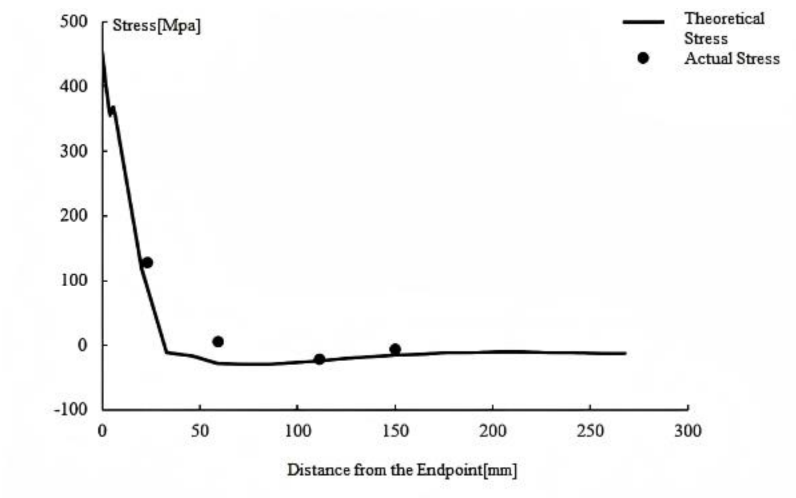

Figure 12: Comparison of U rib residual stress simulation and experimental results

As shown in Fig. 12, the overall variation trend of the simulated stresses is consistent with the experimental measurements. Stress gradually decreases and stabilizes as the distance from the weld joint increases. However, significant discrepancies are observed near the joint (0-50 mm). These differences are primarily attributed to manufacturing effects. During fabrication, the cold-bending process introduces initial residual stresses, which are further superimposed during welding, resulting in measured stresses higher than the theoretical simulation values. With increasing distance from the joint, the simulated and measured values converge, and the measured data are distributed around the simulated curve, indicating good overall agreement.

Although minor deviations exist, the numerical simulation captures the general distribution law of residual stress in the U rib, further confirming the validity and reliability of the stress-field model.

2.6. The results of stress field

In the thermo-mechanical coupling simulation of the top plate-U rib welded structure, thermal shrinkage deformation during the phase-transformation cooling stage leads to the formation of a multiaxial residual stress field. Specifically, longitudinal shrinkage along the weld path generates residual tensile stress in the longitudinal direction due to geometric constraints, while transverse shrinkage perpendicular to the weld induces a transverse residual stress field. For thick-plate welded structures with plate thickness exceeding 6 mm (in this study, the top plate is 16 mm and the U rib is 8 mm), the significant temperature gradient through the thickness renders the residual stress distribution along the thickness direction particularly important.

In this study, a three-dimensional residual stress analysis system was established to investigate the following stress components: (1) Longitudinal residual stress (parallel to the weld direction, denoted as σz); (2) Transverse residual stress (perpendicular to the weld direction, denoted as σx); (3) Thickness-direction residual stress (along the top plate thickness, denoted as σy). By constructing a three-dimensional stress-coupling model, the interaction mechanisms of the multiaxial residual stress field and its influence on structural bearing performance were elucidated. The equivalent stress field after cooling, along with the residual stress distributions in the three principal directions, is shown in Fig. 13.

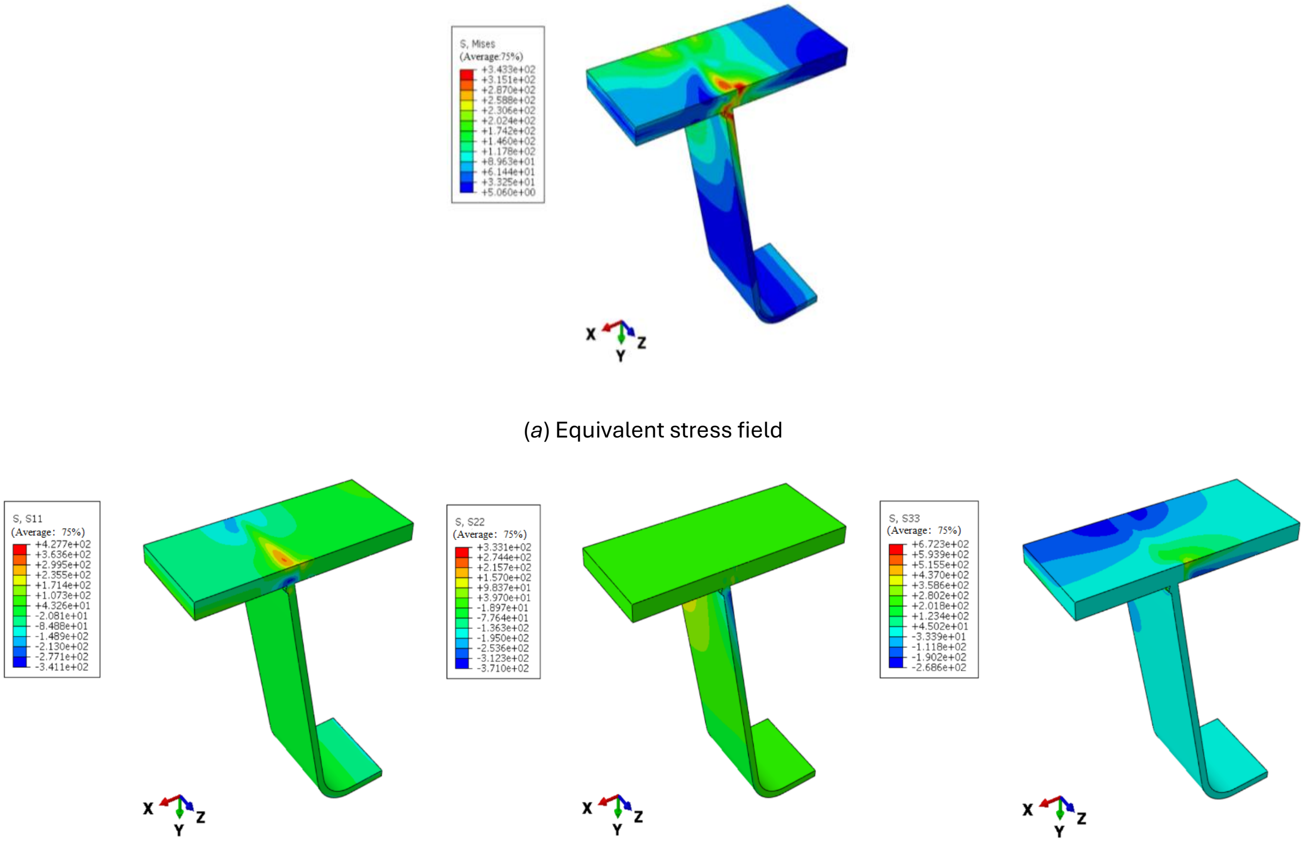

(*a*) Equivalent stress field

(*b*) S_{11} (*c*) S_{22} (*d*) S_{33}

Figure 13: Distribution of different stress fields

Here, S11 represents the direction perpendicular to the weld, S22 represents the top plate thickness direction, and S33 represents the weld direction. As shown in Fig. 13, the peak equivalent stress reaches 343.3 MPa, concentrated in the weld region. The maximum residual tensile stress perpendicular to the weld (S11) is 427.7 MPa, and along the top plate thickness (S22) is 333.1 MPa. In both cases, the peak stresses are located at the junction between the weld seam, the top plate, and the U rib. The longitudinal residual tensile stress along the weld (S33) reaches 672.3 MPa, significantly exceeding the material yield strength. Residual tensile stress is primarily concentrated in the narrow weld seam region, whereas residual compressive stress occurs in areas distant from the weld, with a maximum magnitude of 268.6 MPa. Moving outward from the weld center, residual tensile stress gradually decreases, while residual compressive stress increases correspondingly.

The analysis results indicate that some localized stress concentrations in the S33 direction reach the ultimate strength of the actual material; however, the extracted equivalent von Mises stress shows that the overall stress level of the weld does not exceed the yield strength. To avoid convergence issues caused by the descending portion of the material constitutive curve in the numerical model, the post-ultimate-strain descending segment was not defined in the constitutive curve, and the effect of stress redistribution in individual directions was neglected. This simplification is consistent with previous experimental observations and does not significantly affect the reliability of the simulation results.

3. Analysis of geometry

In this part of the study, the main objective is to investigate how changes in specific component dimensions affect residual stress. The influence of other parameters has been considered in previous sections and will not be discussed further here. The focus is on examining the distribution patterns of longitudinal welding residual stress in the top plate-U rib under the variation of four different geometric parameters.

3.1. Influence of different plate thicknesses on welding residual stress

To investigate the effect of top plate thickness on the gradient distribution of residual stress, four numerical models with different top plate thicknesses (14 mm, 16 mm, 18 mm, and 20 mm) were established while keeping all other welding parameters constant. The correlation between the thickness parameter and the residual stress field was revealed through comparative analysis.

Distribution of top plate residual stress

As shown in Fig. 14, for top plates of different thicknesses, the longitudinal residual stress along the weld direction exhibits a tensile stress peak of approximately 540 MPa at roughly the same position (between 80 and 90 mm). This exceeds the material yield strength, indicating stress concentration occurs in this region under all thickness conditions. Moreover, the peak residual tensile stress increases as the top plate thickness decreases: in the peak region, the stress rises from 510 MPa (20 mm plate) to 550 MPa (14 mm plate). The stress curves on both sides of the peak are nearly symmetric, gradually attenuating with increasing distance from the peak.

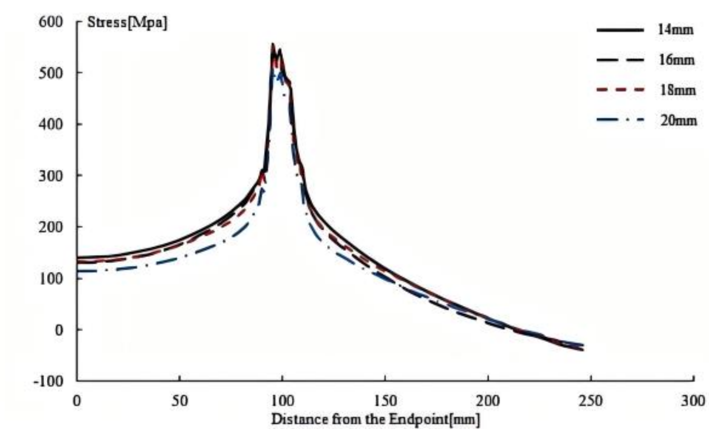

Figure 14: Distribution of longitudinal residual stress in the top plate (S_{33})

Distribution of U rib plate residual stress

Fig. 15 presents the longitudinal residual stress distribution (parallel to the weld direction) in the U rib plate. In the weld central region, the first stress peak occurs at the weld center, reaching 480 MPa, which significantly exceeds the room-temperature yield strength of Q345 steel (345 MPa). A second peak appears within 8-10 mm from the joint, and the magnitude of this peak increases linearly with increasing top plate thickness. In regions farther from the weld seam (beyond 30 mm), the stress state transitions from tensile to compressive. The peak compressive stress occurs at 25-35 mm from the joint. As the distance continues to increase, the compressive stress gradually diminishes, eventually relaxing to approximately 0 MPa at locations far from the weld seam.

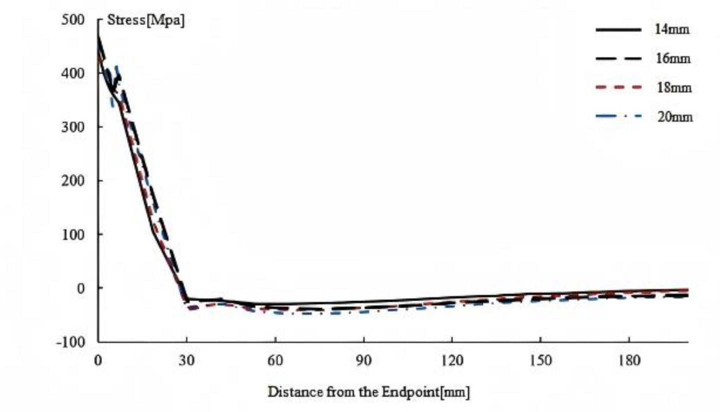

Figure 15: Distribution of longitudinal residual stress in the U rib plate (S_{33})

3.2. Influence of different bevel angles on welding residual stress

In practical welding processes, bevel angles are important dimensional parameters. Selecting an appropriate bevel angle can help reduce residual stress in the top plate-U rib, making its optimization significant for structural design. This study investigates the longitudinal residual stress distribution in the top plate and U rib under four different bevel angles (46°, 48°, 50°, and 52°) at the top plate-U rib joint.

Distribution of residual stress in the top plate

As shown in Fig. 16, the peak longitudinal residual stress in the top plate gradually increases with increasing bevel angle, rising from 455 MPa at 46° to 500 MPa at 52°. However, this trend is less clear in regions farther from the weld seam, where the behavior cannot be definitively determined. Residual compressive stress appears at approximately 200 mm from the start and end of the weld, but its magnitude is minor and can be considered negligible.

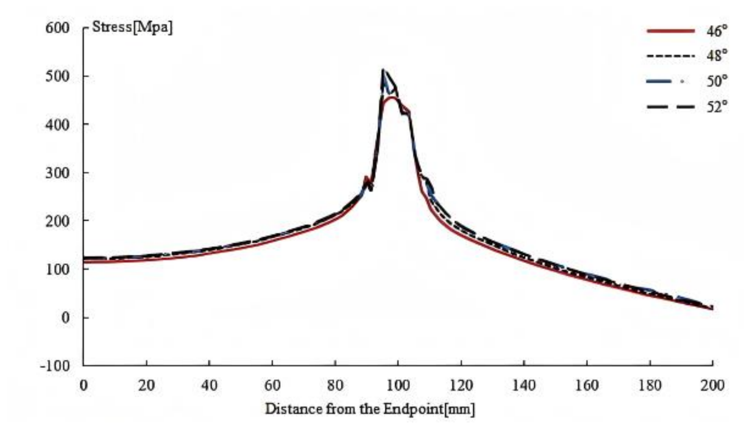

Figure 16: Distribution of longitudinal residual stress in the top plate (S_{33})

Distribution of U rib plate residual stress

Fig. 17 shows that the longitudinal residual stress distribution in the U rib plate exhibits similar trends for all bevel angles. In the peak stress region, the longitudinal residual stress gradually increases with the bevel angle. However, this trend diminishes in regions farther from the weld seam, highlighting the importance of considering bevel angle during welding design to control residual stress.

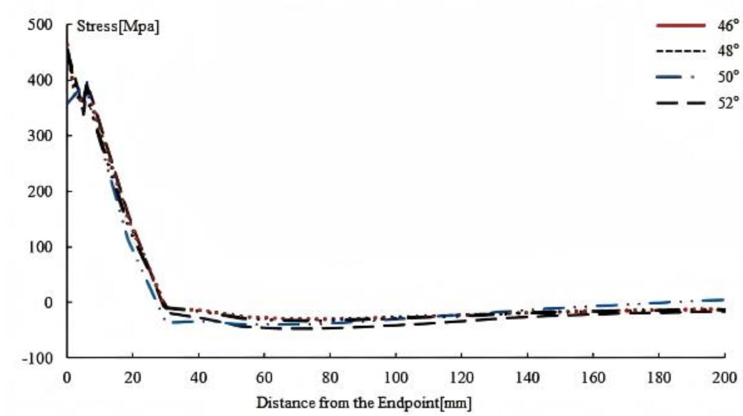

Figure 17: Distribution of longitudinal residual stress in the U rib plate (S_{33})

3.3. Influence of different U rib height on welding residual stress

In the finite element simulation of the top plate-U rib joint, multiple dimensional factors affect residual stress. To comprehensively evaluate the influence of geometric parameters, this section investigates the effect of U rib height. Four U rib heights-270 mm, 280 mm, 310 mm, and 350 mm-were selected, and corresponding models were established to analyze the residual stress fields.

Distribution of top plate residual stress

The distribution of longitudinal residual stress in the top plate under different U rib heights is shown in Fig. 18. The stress patterns for all four U rib heights are generally similar, with peak tensile stress in the weld seam area reaching approximately 500 MPa. Specifically, the peak stress rises from 492 MPa at a U rib height of 270 mm to 520 MPa at 280 mm, but decreases at heights of 310 mm and 350 mm. This indicates that both excessively low and excessively high U rib heights can influence residual stress distribution, and should therefore be considered when designing bridge deck plate-U rib components.

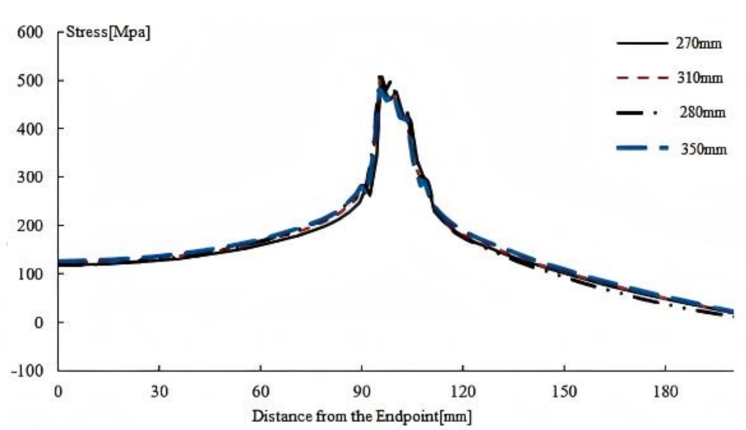

Figure 18: Distribution of longitudinal residual stress in the top plate (S_{33})

Distribution of U rib plate residual stress

Fig. 19 shows the longitudinal residual stress distribution in the U rib plate, which exhibits a trend similar to that observed in the top plate. When the U rib height increases from 270 mm to 280 mm, the peak stress at the weld seam also rises. Conversely, as the height further increases from 310 mm to 350 mm, the peak stress gradually decreases. The residual stress distribution in regions far from the weld seam is less significant and is not discussed in detail here. Comparing the residual stress distributions in the U rib and the top plate highlights the importance of considering U rib height when designing components to control residual stress effectively.

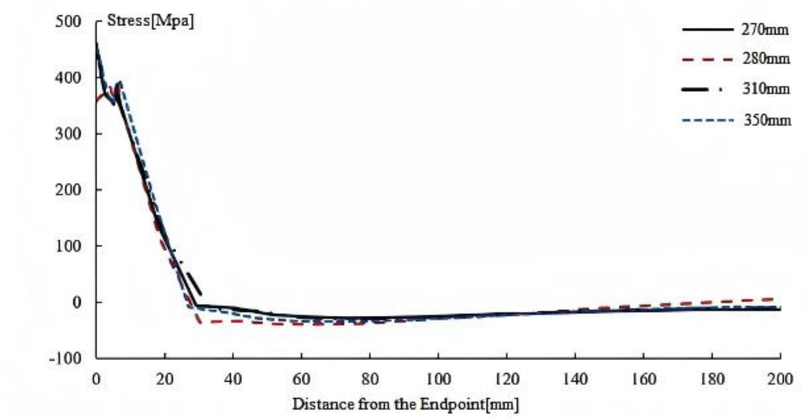

Figure 19: Distribution of longitudinal residual stress in the U rib plate (S_{33})

3.4. Influence of different U rib thicknesses on welding residual stress

The effect of U rib thickness on residual stress distribution is also investigated. Four thicknesses-6 mm, 8 mm, 10 mm, and 12 mm-were selected, and the corresponding residual stress fields were analyzed.

Distribution of top plate residual stress

As shown in Fig. 20, the longitudinal residual stress in the top plate exhibits noticeable differences among U ribs of different thicknesses. All curves display a prominent stress peak at approximately 100 mm, indicating a potential stress concentration region. The peak stresses for the four thicknesses are generally similar, suggesting that variations in U rib thickness have little influence on the maximum stress. Beyond the peak region, the stress gradually decreases with increasing distance and tends to stabilize, likely due to the redistribution and homogenization of internal stresses away from the concentration area.

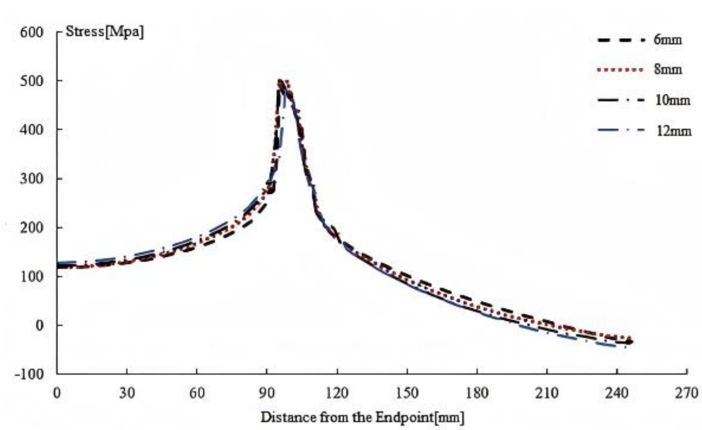

Figure 20: Distribution of longitudinal residual stress in the top plate (S_{33})

Distribution of U rib plate residual stress

Fig. 21 presents the longitudinal residual stress in the U rib plate for the four thicknesses. All curves show that residual stress gradually stabilizes beyond 50 mm from the weld contact area, approaching approximately 0 MPa. In regions distant from the weld, the effect of thickness on stress distribution is minimal and the curves are relatively consistent. U ribs with thicknesses of 10 mm and 12 mm exhibit higher peak stresses near the weld but decrease more rapidly, while the 6 mm U rib maintains slightly higher residual tensile stress farther from the weld. Overall, as U rib thickness increases, the overall level of residual stress decreases and the distribution becomes more uniform, indicating that thicker U ribs can effectively reduce residual stress and smooth the stress gradient.

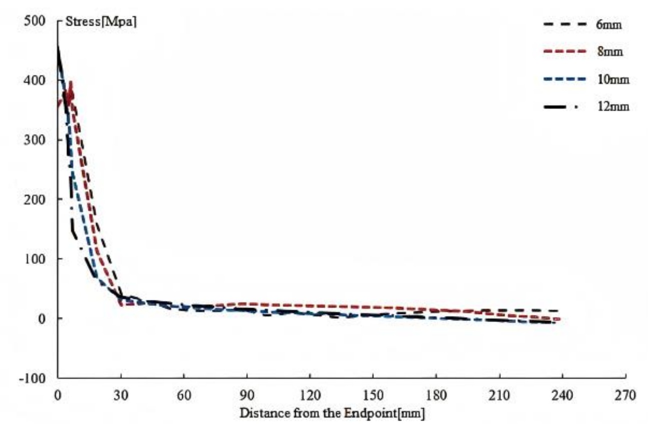

Figure 21: Distribution of longitudinal residual stress in the U rib plate (S_{33})

The influence of U rib thickness on residual stress is primarily concentrated near the weld seam. Thinner U ribs are more prone to higher residual stresses, whereas thicker U ribs can mitigate stress peaks and produce a more gradual stress distribution. Therefore, U rib thickness should be considered a critical parameter when analyzing residual stress in top plate-U rib joints.

4. Regression analysis on the influence of geometric parameters on welding residual stress

During the welding process, variations in geometric dimensions of the test piece can significantly affect the distribution and magnitude of the resulting residual stress field. In the previous section, the influence of four key geometric parameters on welding residual stress was examined, and their effects were illustrated through comparative line charts. Although these charts reveal the basic distribution patterns and qualitative trends of residual stress, such visual observation alone is insufficient for quantitatively determining the relative importance of each parameter.

To address this limitation, the data obtained from the parametric analyses were further processed in this section using SPSS statistical software. A mathematical regression analysis was conducted to identify which geometric parameter exerts the most significant influence on the longitudinal residual stress in the top plate-U rib welded joint. Through this statistical approach, the study aims to provide a more objective and quantitative basis for evaluating parameter sensitivity and guiding structural optimization.

4.1. The steps of regression analysis

Since regression analysis represents only a small component of this chapter, the key procedures are summarized as follows: (1) Define the independent and dependent variables, which is the prerequisite for conducting regression analysis; (2) Establish the mathematical model and determine the regression relationship; (3) Perform iterative computations using SPSS, during which the model may need timely adjustments-this step simultaneously serves as a validation of the model-building process, allowing errors to be identified and corrected promptly; and (4) Verify the regression results, including the t-test, F-test, and goodness-of-fit evaluation. Only after all tests confirm the reliability of the model can credible conclusions be obtained. Figure 22 presents the workflow of the entire regression analysis.

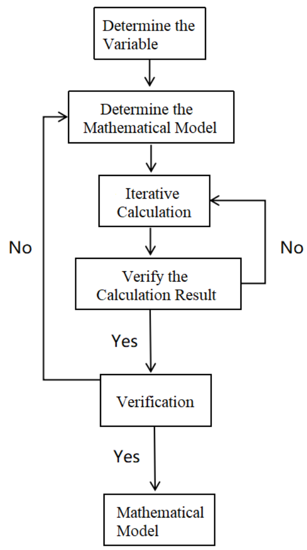

Figure 22: Flow chart of regression analysis

4.2. Design dimensional parameters

Based on the previous subsections, a multiple nonlinear regression model is established to investigate the relationship between four key geometric design parameters and the resulting welding residual stress. First, the longitudinal residual stress at four characteristic moments along the weld direction is identified and summarized. According to the procedures described in Section 2, the residual stress data under the four dimensional parameters are organized, and four sets of eight multiple linear equations are formulated. These four datasets correspond to the moments of 5 s, 10 s, and 12.5 s after the initiation of the second welding pass, as well as the moment when final cooling is completed. Each dataset includes the peak longitudinal residual stress of both the top plate and the U rib, denoted as D1, D2, F1, F2, H1, H2, G1, and G2. Specifically, D1 and D2 represent the peak stresses of the top plate and the U rib at 5 s; F1 and F2 correspond to 10 s; H1 and H2 correspond to 12.5 s; and G1 and G2 represent the final cooling stage. The summarized data are shown in Fig. 23.

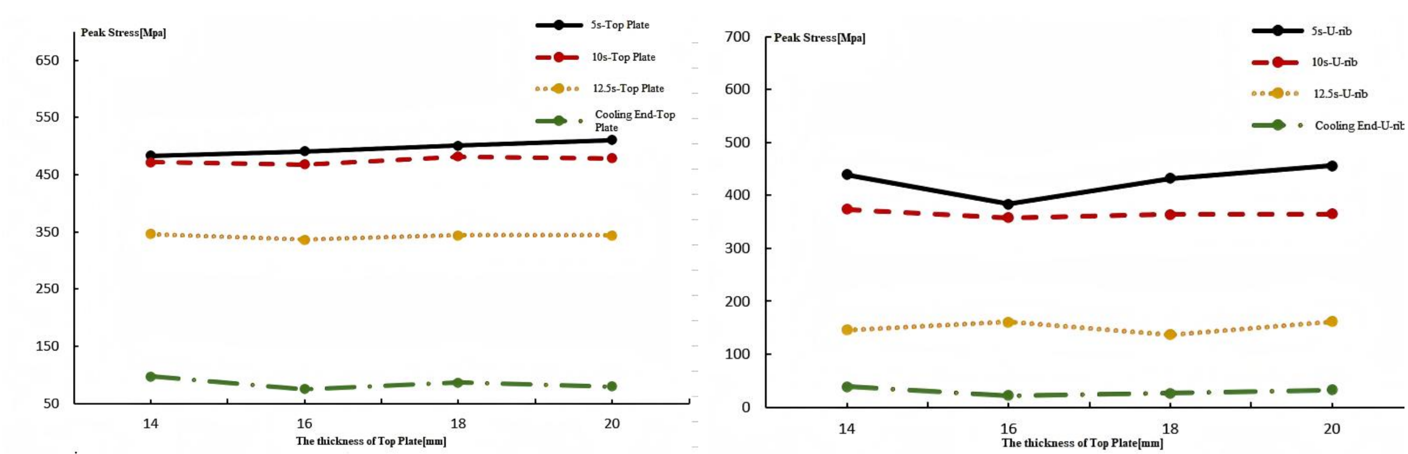

(*a*) Peak stress variation with top plate thickness (top plate) (*b*) Peak stress variation with top plate thickness (U rib)

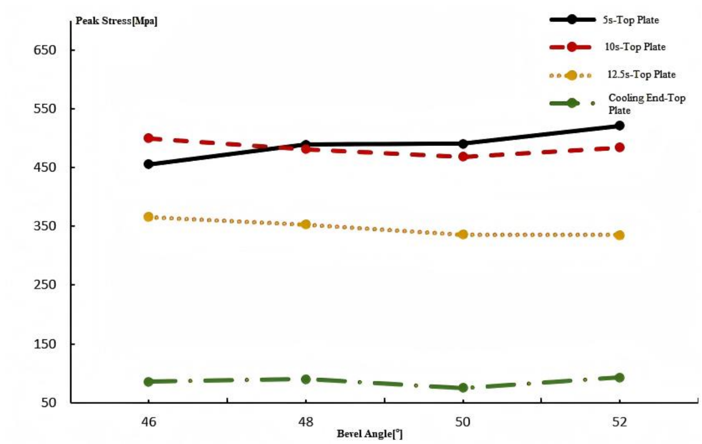

(*c*) Peak stress variation with bevel angle (top plate)

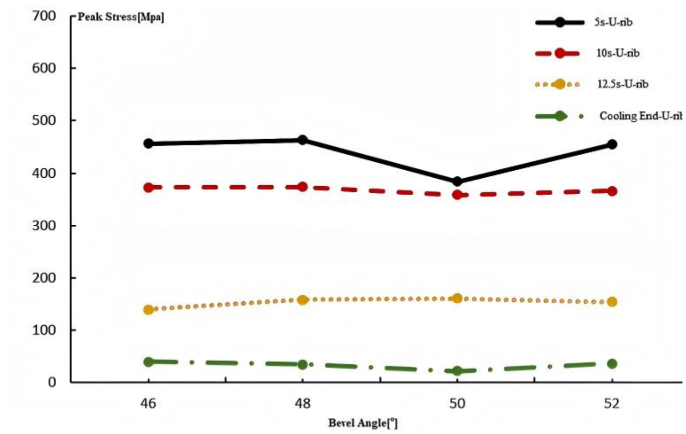

(*d*) Peak stress variation with bevel angle (U rib)

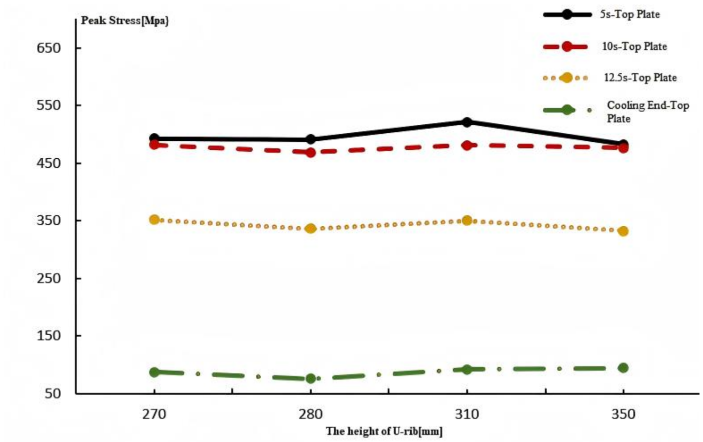

(*e*) Peak stress variation with U rib height (top plate)

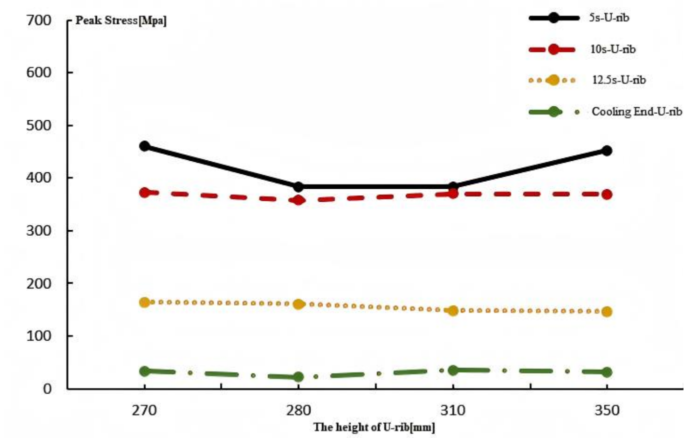

(*f*) Peak stress variation with U rib height (U rib)

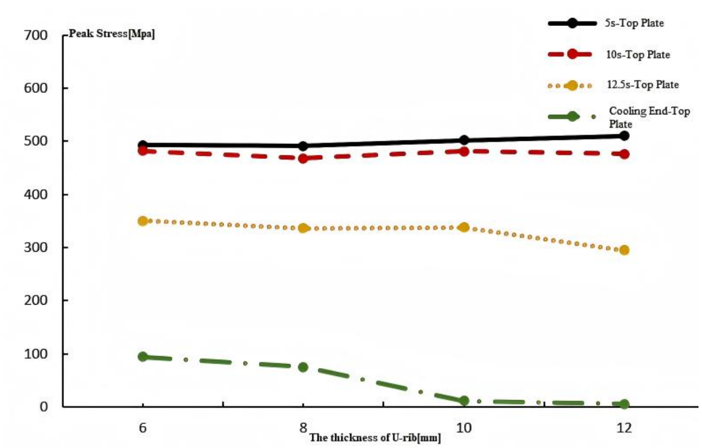

(*g*) Peak stress variation with U rib thickness (top plate)

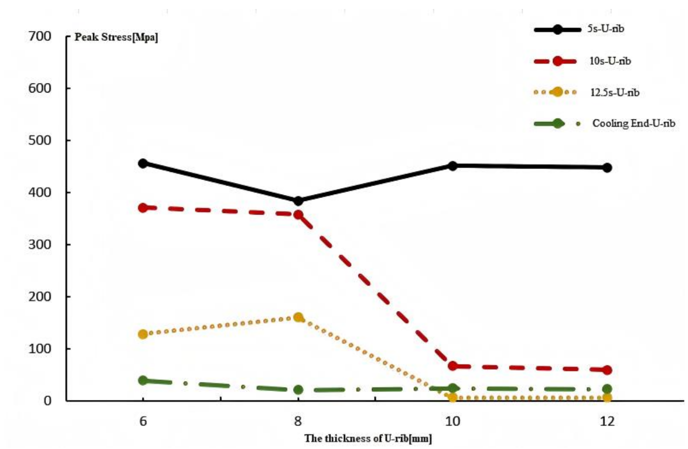

(*h*) Peak stress variation with U rib thickness (U rib)

Figure 23: Peak residual stress variations under different geometric parameters

4.3. Multiple nonlinear regression

A regression analysis is conducted based on the observed values above. Considering the coupling relationships among the dependent and independent variables, the multiple nonlinear regression model is expressed in Equation (1).

$$y = \beta_0 + \beta_1 x_1 + \cdots + \beta_p x_p \sum_{1 \le i,j \le p} \beta_{ij} x_i y_j \quad (1)$$

Where:
x - independent variable,
y - dependent variable,
β - parameter.

To perform the regression analysis, the nonlinear model (Equation 1) must be transformed into a multiple linear regression form. SPSS software is then used to fit the linear regression model, followed by the F-test, t-test, and goodness-of-fit assessment. The linear regression model is shown in Equation (2).

$$R = 12.35 + 0.85a - 0.15b + 0.25c - 0.45d \quad (2)$$

Where:
R - peak stress [MPa],
a - top plate thickness [mm],
b - bevel angle [°],
c - U rib height [mm],
d - U rib thickness [mm].

The calculations are then performed, and the test results are presented in Table 3.

Table 3: Regression analysis results

Items	Non-standardized coefficients		Standardized coefficients	*t*	*p*	Collinearity diagnostics	
	β	Standard error	*Beta*			VIF	Tolerance
Constant [-]	12.35	1.20	-	10.29	0.0065	-	-
Top plate thickness (*a*) [mm]	-0.85	0.05	-0.63	-17.00	0.005	1.5	0.67
Bevel angle (*b*)	0.45	0.08	0.24	4.15	0.018	1.8	0.56
U rib height (*c*) [mm]	0.25	0.03	0.18	1.98	0.045	1.2	0.83
U rib thickness (*d*) [mm]	-0.32	0.06	-0.28	-2.12	0.038	2.0	0.50
R^2 [-]	0.64						
Adjust R^2 [-]	0.61						
F [-]	$F(42.60)=0.756$, $p=0.0065$						

As shown in Table 3, the F is 42.60 with $p=0.0065$, which is far below 0.05. This indicates that the regression model is statistically significant overall, and the combined effects of the independent variables have a significant influence on the dependent variable. The coefficient of determination $R^2=0.64$ suggests that the model explains 64% of the variance in the dependent variable, indicating *a* relatively high explanatory capability. The adjusted $R^2=0.61$ is slightly lower but still demonstrates a strong goodness of fit. The unstandardized coefficient $\beta=12.35$ for the constant term implies that when all independent variables are zero, the predicted value of the dependent variable is 12.35. The relationships for each variable are summarized as follows:

1) The unstandardized coefficient for top plate thickness a is β=−0.85, with a standardized coefficient of Beta=−0.63. The t=−17.00 and p=0.005 indicate that top plate thickness has a significant negative effect on the dependent variable, and the magnitude of its influence is substantial.

2) The unstandardized coefficient for bevel angle *b* is β=0.45, with a standardized coefficient of *Beta*=0.24. The t=4.15 and p=0.018 show that bevel angle exerts a significant positive effect, meaning that peak stress increases as the bevel angle increases. Its influence ranks second among the four parameters.

3) The unstandardized coefficient for U rib height *c* is β=0.25, with a standardized coefficient of *Beta*=0.18. With a *t*=1.98 and *p*=0.045, U rib height has a positive but relatively modest effect on peak stress.

4) The unstandardized coefficient for U rib thickness *d* is β=−0.32, with a standardized coefficient of *Beta*=−0.28. The *t*=−2.12 and *p*=0.038 indicate that U rib thickness has a significant negative effect, though its influence intensity is the weakest among the four parameters.

5. Conclusion

Based on the thermal-mechanical coupling simulation and regression analysis of the top plate-U rib welded structure, several insights into the distribution and influencing factors of welding residual stress can be drawn.

Firstly, the residual stress field exhibits a clear spatial pattern centered on the weld seam. Peak stress occurs near the weld zone and gradually attenuates with increasing distance. In areas far from the weld, the stress state may transition from tensile to compressive, reflecting the complex multiaxial stress interactions induced by welding.

Secondly, the influence of key geometric parameters on longitudinal residual stress was systematically investigated. The main observations are as follows:

1) Top plate thickness: An increase in thickness leads to higher longitudinal residual tensile stress in the weld zone, while the effect on regions distant from the weld gradually diminishes.

2) Bevel angle: Larger bevel angles result in higher peak longitudinal residual stress in both the top plate and U rib, though the influence weakens in distal areas.

3) U rib height: Increasing the height slightly reduces peak stress at the weld seam but has limited effect on the stress distribution in areas away from the weld.

4) U rib thickness: This parameter strongly affects residual stress near the weld; thinner ribs tend to generate higher residual stresses, whereas thicker ribs help produce a more uniform stress distribution.

Finally, regression analysis quantifies the relative importance of these parameters. Top plate thickness has the most significant influence, exhibiting a negative correlation with residual stress, followed by bevel angle, U rib thickness, and U rib height, which shows the weakest effect. These findings indicate that top plate thickness is the primary design factor controlling residual stress in top plate-U rib joints. Based on the simulation results, a top plate thickness of 16-18 mm is recommended in engineering practice to balance structural performance and residual stress mitigation.

Acknowledgements

The financial support from the Natural Science Foundation of Chongqing with Grant No. CSTB2023NSCQ-MSX0654, and the Natural Science Foundation of Chongqing with Grant No. cstc2019jcyj-msxmX0556.

Author Contributions

Y.C. conceived and designed the study. **Q.L.** conducted the experiments and collected the data. **Z.Z.** performed the statistical analysis and manuscript drafting. **P.S.** contributed to data interpretation and Funding acquisition. **W. Q.** manuscript editing. **Y.G.** Formal analysis. All authors critically reviewed and approved the final version of the manuscript and agreed to be accountable for all aspects of the work.

References

McCLUNG, R. C. (2007). A literature survey on the stability and significance of residual stress during fatigue. *Fatigue and Fracture of Engineering Materials and Structures*, 27(1), 173-205. https://doi.org/10.1111/j.1460-2695.2007.01102.x

Tabatabaeian, A., Ghasemi, A. R., Shokrieh, M. M., Marzbanrad, B., Baraheni, M., & Fotouhi, M. (2022). Residual stress in engineering materials: a review. *Advanced engineering materials*, 24(3), 2100786. https://doi.org/10.1002/adem.202100786

Liu, Q., Qiang, B., Xie, Y., Xie, Q., Zou, Y., Yao, C., & Li, Y. (2024). PWHT influence on welding residual stress in 45 mm bridge steel butt-welded joint. *Journal of Constructional Steel Research*, 217, 108674. https://doi.org/10.1016/j.jcsr.2024.108674

Odrobiňák, J., Vičan, J., Hlinka, R., Prokop, J., & Vavák, B. (2025). On the load-carrying capacity determination of railway box-girder bridges using the reduced stress method. *Civil and Environmental Engineering*, 0(0). https://doi.org/10.2478/cee-2026-0021

Van den Berg, N., Xin, H., & Veljkovic, M. (2021). Effects of residual stresses on fatigue crack propagation of an orthotropic steel bridge deck. *Materials & Design*, 198, 109294. https://doi.org/10.1016/j.matdes.2020.109294

Zhang, H., Li, L., Ma, W., Luo, Y., Li, Z., & Kuai, H. (2022). Effects of welding residual stresses on fatigue reliability assessment of a PC beam bridge with corrugated steel webs under dynamic vehicle loading. *Structures*, 45, 1561-1572. https://doi.org/10.1016/j.istruc.2022.09.094

Van Pham, P., Doan-Tan, T., Le-Dang, D. & Xuan-Huy, N. (2024). Inelastic moment resistances of welded steel beams with initial shape imperfections. *Civil and Environmental Engineering*, 20(2), 632-653. https://doi.org/10.2478/cee-2024-0048

Chen, Y., Pan, X., Shen, P., Li, Q., Zhang, Y. (2025). Review of the influential weld details on fatigue failure of OSD in RD joints, *GRAĐEVINAR*, 77 (5), 471-484, doi: https://doi.org/10.14256/JCE.4193.2024

Cui, C., Zhang, Q., Bao, Y., Bu, Y., & Luo, Y. (2019). Fatigue life evaluation of welded joints in steel bridge considering residual stress. *Journal of Constructional Steel Research*, 153, 509-518. https://doi.org/10.1016/j.jcsr.2018.11.003

Gadallah, R., Tsutsumi, S., Yonezawa, T., & Shimanuki, H. (2020). Residual stress measurement at the weld root of rib-to-deck welded joints in orthotropic steel bridge decks using the contour method. *Engineering Structures*, 219, 110946. https://doi.org/10.1016/j.engstruct.2020.110946

Shim, Y., Feng, Z., Lee, S., Kim, D., Jaeger, J., Papritan, J. C., & Tsai, C. L. (1992). Determination of residual stresses in thick-section weldments. *Welding Journal*, 71(9), 305-312.

Wang, K., Jie, Z., Liang, S., & Zhuge, P. (2023). Fatigue assessment of U-rib full penetration welded joints based on local methods. *Journal of Constructional Steel Research*, 200, 107684. https://doi.org/10.1016/j.jcsr.2022.107684

Chen, Y., Shen, P., Li, C., & Zhou, J. (2025). Analysis of the geometrical size effect on the fatigue performance of welded T-joints. *Buildings*, 15(19), 3627. https://doi.org/10.3390/buildings15193627

Liang, S., Jie, Z., & Wang, K. (2022). Numerical simulation and ultrasonic measurement on welding residual stresses of full penetration U-shaped stiffening ribs. *Structures*, 46, 322-335. https://doi.org/10.1016/j.istruc.2022.10.072

Li, X., Fu, Z., Shu, J., Ji, B., & Ji, B. (2024). A modified physics-informed neural network to fatigue life prediction of deck-rib double-side welded joints. *International Journal of Fatigue*, 189, 108566. https://doi.org/10.1016/j.ijfatigue.2024.108566

Bora, A., & Podder, D. (2024). Residual stress reduction through thermo-mechanical tensioning for an orthotropic steel bridge deck. *Journal of Materials Engineering and Performance*, 33(8), 4012-4028. https://doi.org/10.1007/s11665-023-09129-0

Mondal, A. K., Kumar, B., Bag, S., Nirsanametla, Y., & Biswas, P. (2021). Development of avocado shape heat source model for finite element based heat transfer analysis of high-velocity arc welding process. *International Journal of Thermal Sciences*, 166, 107005. https://doi.org/10.1016/j.ijthermalsci.2021.107005

Nascimento, E. J., dos Santos Magalhães, E., & dos Santos Paes, L. E. (2023). A literature review in heat source thermal modeling applied to welding and similar processes. *The International Journal of Advanced Manufacturing Technology*, 126(7), 2917-2957. https://doi.org/10.1007/s00170-023-11253-z

Boussaq, C., Samaouali, A., Belarouf, S., Soulami, H., Ajani, M., Karim, I., Moufakkir, A., Douha, B. & Arbaoui, A. (2025). Experimental analysis of thermal conductivity and volumetric heat capacity in concrete incorporating HDPE waste plastic powder as a function of temperature. *Civil and Environmental Engineering*, 21(1), 2025. 591-604. https://doi.org/10.2478/cee-2025-0045

Djoković, J.M., Nikolić, R.R., & Bujňák, J. (2015). Impact of the weld geometry on the stress intensity factor of the welded T-joint exposed to the tensile force and the bending moment. *Civil and Environmental Engineering*, 11(2), 2015. 103-109. https://doi.org/10.1515/cee-2015-0013

Yu, D., Yang, C., Sun, Q., Dai, L., Wang, A., & Xuan, H. (2023). Impact of process parameters on temperature and residual stress distribution of X80 pipe girth welds. *International Journal of Pressure Vessels and Piping*, 203, 104939. https://doi.org/10.1016/j.ijpvp.2023.104939

Gu, L., Hong, J., & Ma, N. (2024). Analysis and simplified model calculation of residual stress in U-rib welding of steel bridge deck. *Advances in Mechanical Engineering*, 16(7), 16878132241266457. https://doi.org/10.1177/1687813224126

Wang, F., Lyu, Z. D., Zhao, Z., Chen, Q. K., & Mei, H. L. (2020). Experimental and numerical study on welding residual stress of U-rib stiffened plates. *Journal of Constructional Steel Research*, 175, 106362. https://doi.org/10.1016/j.jcsr.2020.106362

Zheng, H., Jie, Z., Zhang, L., & Lu, W. (2024). Fatigue crack growth and life assessment of full penetration U-rib welded joints considering residual stresses. *Thin-Walled Structures*, 195, 111426. https://doi.org/10.1016/j.tws.2023.111426

How to Cite This Article

Chen, Y., Li, Q., Zhang, Z., Shen, P., Qiu, W., & Gu, Y. (2026). Analysis of the Influence of Different Geometric Parameters on Residual Stress of Top Plate-U Ribs. Civil and Environmental Engineering, 0 (0). https://doi.org/10.2478/cee-2026-0073